Accepted Manuscript

AbiEi binds cooperatively to the Type IV abiE toxin-antitoxin operator via a positively-charged surface and causes DNA bending and negative autoregulation

Hannah G. Hampton, Simon A. Jackson, Robert D. Fagerlund, Anne I.M. Vogel, Ron L. Dy, Tim R. Blower, Peter C. Fineran

PII: S0022-2836(18)30107-4
DOI: doi:10.1016/j.jmb.2018.02.022
Reference: YJMBI 65625

To appear in:

Received date: 11 January 2018
Revised date: 24 February 2018
Accepted date: 24 February 2018

Please cite this article as: Hannah G. Hampton, Simon A. Jackson, Robert D. Fagerlund, Anne I.M. Vogel, Ron L. Dy, Tim R. Blower, Peter C. Fineran , AbiEi binds cooperatively to the Type IV abiE toxin-antitoxin operator via a positively-charged surface and causes DNA bending and negative autoregulation. The address for the corresponding author was captured as affiliation for all authors. Please check if appropriate. Yjmbi(2018), doi:10.1016/j.jmb.2018.02.022

AbiEi binds cooperatively to the Type IV *abiE* toxin-antitoxin operator via a positively-charged surface and causes DNA bending and negative autoregulation

Hannah G. Hampton[a], Simon A. Jackson[a], Robert D. Fagerlund[a], Anne I.M. Vogel[a, 1], Ron L. Dy[a, 2], Tim R. Blower[b] and Peter C. Fineran[a]

[a]Department of Microbiology and Immunology, University of Otago, PO Box 56, Dunedin 9054, New Zealand.

[b]Department of Biosciences, Durham University, South Road, Durham DH1 3LE, UK.

[1]Present address: Department of Biotechnology, Norwegian University of Science and Technology, 7491 Trondheim, Norway

[2]Present address: National Institute of Molecular Biology and Biotechnology (NIMBB), University of the Philippines, Diliman, Quezon City, Philippines

Correspondence to Peter C. Fineran: peter.fineran@otago.ac.nz; Tel. +64 (0)3 479 7735; Fax. +64 (0)3 479 8540.

Keywords: toxin-antitoxin system; abortive infection system; phage resistance; AbiE; COG5340

Abbreviations: Abi – abortive infection, β-gal – beta-galactosidase, CTD – C-terminal domain, EMSA – electrophoretic mobility shift assay, IR – inverted repeat,

NTD – N-terminal domain, SDM – site directed mutant, TA – toxin-antitoxin, wHTH – winged helix-turn-helix

Abstract

Bacteria resist phage infection using multiple strategies, including CRISPR-Cas and abortive infection (Abi) systems. Abi systems provide population-level protection from phage predation, via 'altruistic' cell suicide. It has recently been shown that some Abi systems function via a toxin-antitoxin (TA) mechanism, such as the widespread AbiE family. The *Streptococcus agalactiae* AbiE system consists of a bicistronic operon encoding the AbiEi antitoxin and AbiEii toxin, which function as a Type IV TA system. Here we examine the AbiEi antitoxin, which belongs to a large family of transcriptional regulators with a conserved N-terminal winged-helix-turn-helix (wHTH) domain. This wHTH is essential for transcriptional repression of the *abiE* operon. The function of the AbiEi C-terminal domain (CTD) is poorly characterised, but it contributes to transcriptional repression and is sufficient for toxin neutralization. We demonstrate that a conserved charged surface on one face of the CTD assists sequence-specific DNA binding and negative autoregulation, without influencing antitoxicity. Furthermore, AbiEi binds cooperatively to two inverted repeats within the *abiE* promoter and bends the DNA by 72°. These findings demonstrate the mechanism of DNA binding by the widespread family of AbiEi antitoxins and transcriptional regulators can contribute to negative autoregulation.

Graphical abstract

Introduction

Bacteriophages (phages) are ubiquitous biological entities, numbering >10^{30} and participating in ~10^{25} infections every second, which affects both bacterial evolution and global carbon cycles [1,2]. In response to these viral threats, bacteria have developed multiple resistance strategies, including CRISPR-Cas 'adaptive immunity' and abortive infection (Abi) 'innate immunity' [3,4]. Like many phage resistance mechanisms, Abi systems function post-infection, typically interfering with phage replication. What sets Abi systems apart from other defences is that their activation results in the death of the infected bacterium – a form of 'bacterial apoptosis' [4,5]. This cell death, which is sometimes viewed as 'altruistic cell suicide', provides community-level protection by limiting the spread of phages through spatially structured bacterial populations [5,6]. Greater than 20 Abi systems have been identified and are predominantly plasmid-encoded in industrially-important lactococci. However, for most Abi systems the molecular basis of phage resistance remains unknown [5] .

Recently, several Abi systems have been shown to act via a toxin-antitoxin (TA) mechanism [7-9] and likewise, some TA systems provide defence against phages [10,11]. Toxin-antitoxin (TA) systems were originally identified on plasmids, where they enhance maintenance by killing cells that lose the plasmid through mis-segregation upon cell division [12,13]. TA systems require the activity of a toxin and an antagonistic antitoxin. Antitoxins are more labile than their cognate toxins and, when synthesis of both ceases (e.g. post-segregation or during phage infection), the antitoxin is quickly degraded, enabling the toxin to affect its target. For all known TA systems, the toxin component is a protein that targets essential cellular processes,

such as DNA replication through inhibition of DNA gyrase (e.g. CcdB) and inhibition of translation by cleavage of mRNAs that are either free (e.g. ToxN) or bound to the ribosomal A-site (e.g. RelE) [3,14,15]. Based on the mechanism of antitoxicity, six types of TA systems have been defined [15,16]. Type I encode small antisense RNAs that interact directly with the toxin mRNA and typically inhibit toxin translation (e.g. Hok-Sok) [12,17]. In Type II, a protein antitoxin inhibits the toxin by directly binding and forming an inactive TA complex (e.g. MazEF) [17-19]. An RNA antitoxin interacts directly with the toxic protein in Type III systems, of which ToxIN is the defining member [8,20]. Type IV are composed of protein toxins and antitoxins that do not directly interact, rather the antitoxin antagonises the toxic activity on the target (e.g. CbeA-CbtA) [7,21,22]. In the Type V GhoST system, a protein antitoxin degrades the toxin transcript, preventing toxin translation [23]. Finally, in the Type VI system, the SocA antitoxin promotes degradation of the SocB toxin by ClpXP [24].

AbiE, from the group B *Streptococcus agalactiae* V/R 2603 is an Abi system that functions via a TA mechanism involving two proteins. It is encoded by a bicistronic operon, with the antitoxin and toxin genes overlapping by 4 bp. The first AbiE system was identified in *Lactococcus lactis* where it aborts ϕc2 and ϕ712 phages of the *Siphoviridae* family [25]. AbiE is a Type IV TA system as there is no apparent direct interaction between the antitoxin, AbiEi, and toxin, AbiEii [7]. The antitoxin and toxin are members of abundant protein families that are most commonly encoded from the same operon (some homologues are wrongly annotated as AbiGi and AbiGii, respectively) [7]. The AbiEii toxin is a putative nucleotidyltransferase (DUF1814) that specifically binds GTP. It is hypothesised that this GTP is transferred to a conserved cellular target(s) of the toxin, but the mechanism of toxicity remains unresolved [7]. DUF1814 proteins are widespread with >3000 identified, although not all encoded

adjacent to a putative antitoxin [7,26,27]. The AbiEi Pfam clan (CL0578) contains three members; AbiEi_4 (e.g. AbiEi [7]), AbiEi_3 (e.g. MosAT [28]) and AbiEi_1 (e.g. Rv2827c [29]), which are present in >600 species of bacteria and archaea.

AbiEi functions as both the antitoxin and a transcriptional repressor of the *abiE* operon [7]. It is composed of an N-terminal domain (NTD) with a conserved wHTH DNA binding motif and a CTD containing a protein fold that has not yet been functionally characterized [7,29]. Autoregulation is common amongst Type II TA systems and can be either positive or negative [30,31]. Antitoxins from Type II TA systems can partially repress operon expression by binding to operators in the promoter region, with full repression being achieved when a complex of the antitoxin and toxin bind through a mechanism termed conditional cooperativity [32]. Such Type II antitoxins commonly have a structured N-terminal DNA-binding motif and a less structured C-terminus that interacts with the toxin [32]. Previous work on the *S. agalactiae* AbiE system revealed that full length AbiEi, is necessary for *abiE* repression, yet the CTD alone is sufficient for inhibition of toxicity [7]. No further repression is seen upon addition of the toxin, showing that the mechanism of autoregulation for this Type IV TA system is different to what is typically observed for conditional cooperativity in Type II TA systems [7].

AbiEi is the first example of a Type IV antitoxin that regulates the expression of its own operon. Here, we demonstrate that a conserved positive surface charge on one face of the CTD is required to stabilize the interaction between AbiEi and the operator sites in the *abiE* promoter, and this occurs through base specific interactions with the DNA. However, this positive surface charge is not required for antitoxic activity. The binding of two AbiEi subunits to the operator inverted repeats

(IRs) is cooperative and involves changes in DNA topology upon binding. Thus, the widespread fold that constitutes the CTD represents a dual-function domain that can provide antitoxicity, while also playing an important role in DNA binding and transcriptional repression.

Results

AbiEi has a conserved positively charged surface predicted to aid DNA binding

AbiEi is predicted to be composed of two functional domains: an N-terminal wHTH DNA-binding motif and a bifunctional CTD important for both promoter repression and toxin neutralization [7]. To investigate the dual functionality of the CTD, we used Phyre2 [33] to search for *S. agalactiae* AbiEi homologues with known structures. The top scoring candidate (98.2% confidence) was Rv2827c from *Mycobacterium. tuberculosis* (Fig. 1a), which provided a structural model for residues 4 to 155 (out of 196) of *S. agalactiae* AbiEi (Fig. 1b). Rv2827c and AbiEi are members of the abundant COG5340 protein family and contain a conserved wHTH DNA-binding domain and a CTD with an arrangement of α-helices and β-sheets forming a unique topology [7,29]. Structural searches using just the CTD revealed that Rv2827c is the only solved protein containing this fold [29]. One face on the CTD of Rv2827c contains a patch of positive charge, which has been proposed to facilitate interaction with DNA (Fig. 1a) [29]; however, there is currently no experimental evidence to support this. A similar positively charged face was present in the *S. agalactiae* AbiEi model, suggesting this is a conserved feature of COG5340 family proteins (Fig. 1b). We identified 18 potential DNA-binding surface-exposed lysine and arginine residues in both the wHTH domain and the positively charged face of the CTD (Fig. 1c-e).

Aligning the wHTH domain of AbiEi with a model of Rv2827c bound to DNA [29] clearly demonstrated the close proximity of the positively charged face of the CTD to the DNA. We theorized that this charged surface would aid the AbiEi-operator site interaction to elicit autoregulation of the *abiE* operon (Fig. 1e).

The positively charged surface cumulatively aids negative autoregulation

To test the hypothesis that the positive surface charge of the CTD assists in interaction of AbiEi with inverted repeats within the *abiE* promoter, we mutated each of the surface-exposed DNA-facing lysine and arginine residues to alanine. A further 7 residues in the C-terminal region that could not be confidently modeled with the Rv2827c template were also mutated (i.e. K159, K169, K170, K174, K181, K187 and K189). The site-directed mutants (SDMs) shown in Fig. 1c-e were tested for their ability to repress expression of the *abiE* operon using a *lacZ* reporter system. The *abiE* promoter region contains a perfect 11 bp palindromic repeat, which can be extended up to 23 bp with only 4 mismatches (Fig. 2a) [7]. Binding of AbiEi to these inverted repeats represses expression of the reporter gene via a negative autoregulation mechanism, resulting in a decrease in β-galactosidase activity (Fig. 2a and b). Wild type (WT) AbiEi inhibited expression from the *abiE* promoter by ~20-fold compared with an empty vector negative control lacking AbiEi (Fig. 2a and b). In wHTH proteins, the protruding recognition helix, most commonly helix 3 (H3), is embedded in the major groove of target DNA through many base-specific contacts [29,34,35] and the wing provides an interface that interacts with the minor groove [36]. As expected, mutation of the critical invariant H3 residue R35 (Fig. 1c) resulted in an almost complete loss of promoter repression, demonstrating the capability of the assay to detect mutants impaired in autoregulation (Fig. 2b). However, no major

impairment in autoregulation was observed for any of the other SDMs. We also examined whether mutation of these positively charged residues affected the ability of AbiEi to antagonise the toxicity of AbiEii, but did not detect any differences compared with the WT antitoxin (Fig. 2d and e). Therefore, these individual charged residues do not play a role in the antitoxicity function of AbiEi and another region of the CTD must be responsible for antitoxicity. Furthermore, because the CTD is required for antitoxicity [7], these results confirm that the mutations did not detectably impair folding or stability of the AbiEi protein.

The lack of impaired negative autoregulation for any of the CTD SDMs led us to hypothesize that the surface charge might function redundantly or cumulatively and hence, not be sufficiently disrupted in these single mutants. We therefore constructed a series of double and triple SDMs to more substantially deplete the net positive charge on the surface of the CTD. As before, residues chosen for mutation were based upon the CTD face predicted to interact with DNA in the AbiEi model (Fig. 1), and also residues in the C-terminus that had not been possible to confidently model. Several double mutants, R44A:R66A, R44A:R100A, R66A:R100A, R97A:R100A, and a R44A:R66A:R100A triple mutant displayed impaired *abiE* repression compared with the corresponding individual SDMs (Fig. 3a). R44 is located within the wing of the wHTH NTD (Fig. 1c and d), residues R66, R97 and R100 are exposed on the CTD surface and lie within close proximity to modelled DNA (Fig. 1e). Therefore, the loss of autoregulation by R44A:R66A, R44A:R100A, R66A:R100A, R97A:R100A and R44A:R66A:R100A suggests that the successive loss of positive charge within certain spatial regions of the CTD surface has an additive effect resulting in a loss of promoter repression. The K69A:R97A, K69A:R100A mutants were moderately impaired in promoter repression (Fig. 3),

therefore the K69 sidechain, which is close to one side of the predicted charged CTD face, appears to contribute to the interaction of AbiEi with the promoter DNA, albeit less than the surface-exposed arginine residues on this face. In contrast, multiple mutations of the far C-terminal lysine residues (i.e. K159A:K170A, K170A:K181A, K181A:K189A, and K170A:K181A:K189A) did not influence autoregulation, indicating that the unmodeled portion of the CTD is not involved in interaction with the *abiE* operator. All AbiEi mutant variants were apparently correctly folded and stable, as mutations of multiple positively charged residues had no effect on antitoxicity (Fig. 3b). Thus, the positively charged residues contribute to a net charge on the AbiEi surface that is important for autoregulation but do not contribute to antitoxicity.

AbiEi binds cooperatively to two inverted repeats overlapping the *abiE* promoter

The impaired ability of AbiEi mutants with depleted surface charges to negatively autoregulate the *abiE* promoter was likely due to reductions in their binding affinity for the *abiE* operators. To test this, we required a quantitative and detailed understanding of how WT AbiEi binds the two operators. Therefore, we performed electrophoretic mobility shift assays (EMSAs) using a 175 bp fluorescently labeled DNA probe containing 100 bp of the sequence upstream of the *abiE* operon, including both inverted repeats. WT AbiEi produced two discrete shifts (Fig. 4a). The binding was specific, as it could be outcompeted by addition of 100-fold excess unlabeled specific, but not non-specific, DNA (Fig. 4a). These single and double shifts likely represent occupancy of either one or both of the inverted repeat sites, respectively. Indeed, replacement of either IR1 or IR2 with cytosines resulted in only

single shifts, indicating that the second binding site had been disrupted (Fig. 4b, c and Fig. S1). No shift was detected when both inverted repeats were replaced with cytosines (Fig. 4d), further confirming the specificity of AbiEi for the inverted repeats. The binding of AbiEi has an apparent dissociation constant (*Kd*) of 10.8 ± 0.7 nM (Fig. 4e). The binding of AbiEi to the *abiE* operators exhibited strong positive cooperativity, which was determined via a Hill plot (n_H = 2.3 ± 0.2; where a slope greater than one indicates cooperativity) (Fig. 4f). Cooperative binding was further supported by analysing the data using a Scatchard plot, where an inverted concave curve indicated cooperativity (Fig. 4g). Thus, AbiEi binds in a specific and cooperative manner to the two inverted repeats in the *abiE* promoter region.

Cooperative binding by AbiEi results in DNA bending

To further characterise the cooperative binding phenotype of AbiEi, we examined the role of the topology of the inverted repeat DNA. Firstly, one inverted repeat is sufficient for non-cooperative AbiEi binding, as a shift was detected using a fluorescent probe consisting of only a single 23 bp IR, demonstrating that no flanking DNA is required (Fig. 4h). Previous work has shown similar 23 bp inverted repeats, separated by three bp are found upstream of other AbiE loci [7]. To show whether the three bp spacing between the two inverted repeats was important for AbiEi binding, we tested the effect of insertion of a 50 bp spacer sequence between the inverted repeats. Using this IR1-spacer-IR2 probe, two discrete shifts were still observed (Fig. 4i). Whilst the *Kd* (8.9 ± 1.4) remains similar to that of the WT probe (Fig. 4j), a decrease in apparent cooperativity was observed (Fig. 4k and l). Nonetheless, the maintenance of some cooperativity, despite the addition of the 50 bp spacer between the operator sites, suggests that a conformational change or

spatial rearrangement in the DNA, such as DNA bending to loop out the intervening space, occurs upon AbiEi binding. To investigate this, we performed DNA bending EMSAs by varying the position of the WT IR1-IR2 operator region along a series of 170 bp probes (Fig. 4m). Greater retardation of the DNA fragment mobility was observed when the operator region was positioned at the centre, compared to near either end of the DNA probes. In the absence of AbiEi, all DNA probes migrated similarly regardless of the operator region location, demonstrating that there is no intrinsic bending or difference in migration of the DNA probes themselves. The relative mobilities of the DNA fragments with and without AbiEi bound, and the position of the AbiE operator region along the probes, was used to calculate that AbiEi induced a 72° ± 2° bend in the operator DNA (Fig. 4n). In summary, AbiEi binds specifically to the two inverted repeats found in the promoter region of the AbiE operon. This binding is strongly cooperative when the operators are appropriately spaced and results in a bend of 72° in the DNA.

The positively charged surface residues on AbiEi increase DNA binding affinity

Several AbiEi variants with single alanine substitutions in amino acids that were predicted to interact with DNA (Fig. 1), were purified and tested for their ability to bind to the *abiE* promoter *in vitro*. When R35 was mutated to alanine, no discreet shift was detected, and consequently the *Kd* could not be determined (Fig. 5a and Fig. S2). This is in agreement with the autoregulation assay data (Fig. 2b), further indicating that there is no stable interaction between AbiEi R35A and the IRs. The single mutation of R66 to alanine resulted in no detectable change in binding affinity to the *abiE* promoter region (Fig. 5a and Fig. S2), indicated by a *Kd* of 8.8 ± 0.6 nM

(Fig. 5a and Fig. S2). Mutation of K47 and K69 to alanine resulted in decreased binding to the *abiE* promoter region, with *Kd* values of 21.9 ± 6.5 and 15.4 ± 4.3, respectively (Fig. 5a). These K47A and K69A variants retained cooperative binding, as determined through Hill and Scatchard plots (Fig. S2). Similarly, the R97A variant had an apparent decrease in binding affinity with a *Kd* of 14.4 ± 1.7, and binding remained cooperative (Fig. 5a and Fig. S2). The R44A and R100A mutants exhibited *Kd* values of 19.2 ± 4.4 nM and 9.6 ± 0.6 nM, respectively and retained cooperativity (Fig. 5a and Fig. S2). However, little or no discrete single shift products were detected (see next section). Therefore, mutation of some single charged amino acids resulted in reduced binding affinities of AbiEi to the WT *abiE* operator sites.

Because the *in vivo* autoregulation experiments demonstrated that repression was decreased with successive mutations on the positive surface of AbiEi (Fig. 3), we hypothesized that these proteins would be attenuated for binding to the WT *abiE* operator. In agreement, R44A:R66A, R44A:R100A and R66A:R100A variants resulted in no DNA binding, indicating that a severe reduction in the positive charge reduces the stability of the AbiEi interaction with the operator (Fig. 5b). When compared with the single amino acid variants (Fig. 5a), these results further support that multiple positively charged residues have a cumulative effect on DNA binding. In summary, the positively charged surface of the CTD stabilizes the interaction of individual AbiEi proteins with the operator DNA leading to negative autoregulation of the *abiE* operon.

The AbiEi CTD binds the extended region of the inverted repeats

To further characterize AbiEi DNA binding, we examined select single mutants in further detail. The R44A and R100A mutants resulted in unique DNA binding profiles,

with no discreet single shifts detected, but an apparent double shift relating to two bound AbiEi proteins occurred (Fig. 5a). To investigate the AbiEi R100A and DNA complex further, we tested R100A using DNA probes in which either one of the two IRs were replaced with cytosines (Fig. 5c). In both cases, no discreet shift was observed, indicating that the mutated protein only formed a stable interaction with the native *abiE* operator that contains both IRs. The Hill and Scatchard plots (Fig. S2) demonstrated that DNA binding by R100A retained cooperativity, despite the inability to form a stable complex with a single IR (Fig. 5c). Therefore, the R100A mutant exhibits obligatory cooperative binding to the *abiE* operator, i.e. occupancy of a single inverted repeat is unstable. The obligate cooperative behaviour of AbiEi R100A was not the result of an altered stoichiometry in solution, because the size exclusion chromatogram was indistinguishable from the WT (Fig. S3). When compared with molecular weight standards, both proteins eluted later than a 29 kDa standard, indicating that AbiEi WT and R100A (27 kDa) are monomers in solution (Fig. S3).

We also selected the R97A mutant that displayed reduced DNA binding affinity, but had cooperative binding similar to WT AbiEi (Fig. 5a). When binding of R97A to DNA containing either of the two IRs replaced with cytosines was tested, a strong discrete shift was detected only when IR2 was present (Fig. 5d). There are four differences between the sequences of the extended 23 bp IRs, all which lie within the extended central regions (Fig. 2a; red bases). This suggests that R97 contributes to base-specific contacts with the extended central regions in the IRs, because when R97 is mutated to alanine it retains binding to IR2 but has a severely reduced affinity for IR1.Therefore, the orientation of AbiEi binding on the IRs involves the wHTH

domains on the conserved outer IR regions and the CTD (which contains the R97 residue) facing each other in the central region of the extended IRs.

Discussion

Here we have revealed the negative autoregulation and DNA binding mechanism used by the AbiEi antitoxin. This is the first example of autoregulation in a Type IV TA system. Based on our data, we propose a model where the wHTH domain of AbiEi binds to the highly conserved external 11 bp of the inverted repeat and the positively charged CTD interacts with the remaining imperfect 12 bp palindrome to stabilize the AbiEi-DNA interaction (Fig. 6). Binding of the first AbiEi monomer to either IR1 or IR2 acts cooperatively to increase the binding of a second AbiEi monomer to the unoccupied IR. When AbiEi is bound to both inverted repeats the operator region is bent by 72°. We propose that DNA bending improves the position of the positively charged face of the CTD for better contact with the inverted repeats. It is also possible that the DNA bending assists in protein-protein interactions between the AbiEi CTDs to contribute to cooperativity. The net effect of AbiEi binding and DNA bending is blocking access of RNA polymerase to the promoter resulting in repression of *abiE* operon expression.

Most current examples of TA regulation are from Type II systems, which typically involves the antitoxins (sometimes in complex with their cognate toxins) binding via their DNA-binding NTDs to IR-based operator sequences within the promoter region, to repress transcription [30-32,37]. A similar N-terminal DNA binding domain (i.e. the wHTH) is observed in the Type IV AbiE system, yet the additional requirement of the AbiEi CTD in both negative autoregulation and antitoxicity makes this system unique. Inverted repeats are present upstream of other AbiEi homologues, indicating they

are a conserved feature of AbiE systems [7]. For example, upstream of *rv2827c* in *M. tuberculosis* we identified 24 bp near-identical inverted repeats separated by 13 bp. Autoregulation of Type II systems is important for maintaining the cellular ratios of toxin to antitoxin [15] and it is likely that the Type IV AbiE negative autoregulation fulfils a similar function.

DNA bending is likely to contribute to the cooperativity observed for AbiEi binding to the *abiE* promoter region. Similarly, autoregulation by the Type II TA system HipBA results from a complex of antitoxin and toxin, binding to four operator regions upstream of the *hipBA* operon and inducing a 70° bend. This bending results in better alignment of the recognition helices, which is proposed to aid HipBA cooperative binding to additional operator regions [38]. Therefore, we propose that DNA bending by AbiEi facilitates the observed cooperativity. In addition, cooperativity might involve protein-protein interactions, and although the structure of the *M. tuberculosis* Rv2827c AbiEi homologue did not reveal a dimerization interface [29], the region in the extreme CTD that could not be confidently modelled may contribute. The obligate cooperativity of R100A (and R44A) suggests that when both inverted repeats are occupied by AbiEi, their interaction is further stabilized, by bending of the operator DNA. Because cooperativity was not altered in other SDMs, the positive charge is not the main factor contributing to cooperativity. In addition, nucleotide-specific interactions are occurring, due to the observed differences in AbiEi R97A stability with the two IRs. High resolution structures of AbiEi in solution and in complex with single or double inverted repeats are required to fully resolve the basis for precise protein:DNA and potential protein:protein interactions.

It is noteworthy that Type IV TA systems do not involve direct interaction of the

antitoxin and toxin [7,21]. For instance, the outcome of Type II TA autoregulation often depends on the antitoxin to toxin ratio and the strength of repression is defined by differences in binding affinities of the antitoxin alone or complexes of antitoxin and toxin [16,39]. In this process of conditional cooperativity, high levels of toxin can then destabilize repression by disrupting cooperativity, causing derepression and reestablishment of antitoxin to sequester the excess toxin [30,40]. As might be expected for Type IV TA systems, where the toxin and antitoxin do not interact [22], AbiEii toxin expression caused no further repression of the *abiE* promoter in the presence of AbiEi [7]. Thus, it appears that the CTD of AbiEi has evolved dual functionality to assist in the cooperative autoregulation of the *abiE* operon whilst also fulfilling its other role as an antitoxin.

Recently, antitoxins from Type II TA systems were shown to regulate the expression of additional genes, outside their own operons, such as those involved in biofilm formation [41-43]. Therefore, it is possible that analogous physiological and metabolic regulation is provided by *S. agalactiae* AbiEi and related Type IV homologues. In support of this, the Rv2827c homologue in *M. tuberculosis* is important for cell replication [44], and its expression is upregulated upon exposure to the first line *M. tuberculosis* drugs isoniazid and streptomycin, and during starvation conditions [45]. The *S. agalactiae abiE* operon resides on an integrative and conjugative element (ICE*Sa2603rplL*) that encodes genes for both metal resistance and virulence [46]. In addition to providing phage resistance, AbiE is likely to have a role in maintenance of this pathogenicity island similar to MosAT in *Vibrio cholerae* [7,28]. AbiE family members are widespread, not just amongst clinically relevant species but throughout almost all bacterial clades. Therefore, it is likely that the classical TA function (stabilisation of mobile genetic elements), Abi system function

(phage resistance) and antitoxin-facilitated physiological regulation provided by AbiE proteins contributes significantly to shaping the physiology and evolution of many bacteria.

Materials and Methods

Bacterial strains and culture conditions

Escherichia coli strains DH5α and BL21 were grown at 37°C in lysogeny broth (LB) with shaking at 200 rpm or on LB containing 1.5% (w/v) agar (LBA). When relevant, media were supplemented with the following antibiotics and supplements: 100 µg/ml ampicillin (Ap); 50 µg/ml kanamycin (Km); 10 µg/ml tetracycline (Tc); 50 µg/ml streptomycin (Sm); 0.1% (w/v) L-arabinose (ara), 0.2% (w/v) D-glucose (glu) and 10 µM isopropyl-β-D-thiogalactopyranoside (IPTG). Bacterial cell density was measured in a Jenway 6300 spectrophotometer at 600 nm (OD_{600}).

Structural modeling and sequence analysis

DNA sequence analyses were performed using Geneious 9.0.5 software [47] and BLAST (nucleotide and protein) [48] was used for sequence identification. A structural model of AbiEi was generated using Phyre2, based on the PDB:1ZEL template [33]. To assist in selection of mutants, we aligned the AbiEi model with a template model of DNA-bound Rv2827c kindly provided by Manfred Weiss [29]. Protein structure coordinate files were obtained from the Protein Data Bank (PDB) (http://www.rcsb.org/pdb) and visualized using PyMOL (http://www.pymol.org). The solvent-accessible electrostatic surface potential was calculated using APBS [49].

DNA isolation and manipulation

All oligonucleotides used are outlined in Table S1. Plasmid DNA was isolated using the Zyppy Plasmid Miniprep Kit (Zymo Research). All plasmids are listed in Table 1 and were confirmed by DNA sequencing. Restriction digests, ligations, transformation of *E. coli* and agarose gel electrophoresis were performed by standard techniques (Sambrook *et al.*, 1989). DNA from PCR and agarose gels was purified using the Illustra GFX PCR DNA and Gel Band Purification Kit (GE Healthcare). Restriction enzymes and T4 ligase were from Roche or New England Biolabs.

***abiE* promoter activity assays**

E. coli strains carrying plasmids expressing the various AbiEi mutants were transformed with a plasmid containing ~200 bp of promoter sequence fused to a *lacZ* reporter gene (pRLD32). Strains were grown in 1.2 ml of LB with appropriate antibiotics within individual wells of Labcon deep 96 square well plates. Plates were incubated with 12,000 rpm shaking at 37°C using a microplate shaker (IncuMix, BioProducts). Expression analysis was performed using the fluorogenic β-galactosidase substrate: 4-Methylumbelliferyl-D-galactoside (MUG) [50,51]. Samples of 100 μl were extracted at specific time points and frozen in separate 96-well microtiter plates at −80°C. Samples were defrosted by incubation at 37°C for 10 min. Ten μl volumes of each sample were subsequently frozen at −80°C and immediately prior to the assay thawed for 10 min at 37°C. During this time the final reaction buffer (PBS, 2 mg/ml lysozyme, 250 μg/ml MUG) was prepared, from which 100 μl was added to the thawed samples. The relative change in fluorescence was immediately monitored using a Varioskan Flash Multimode Reader (Thermo Fisher Scientific)

according to the following parameters: excitation 365 nm, emission 455 nm, 37°C, 8 reads per well, measured every 1 min for 30 min. Relative fluorescent units (RFUs) per second were calculated using the linear increase in fluorescence which was normalized to the OD_{600} of the sample ($RFU/s/OD_{600}$). β-gal activity was normalized to the native promoter activity (at 100%).

Toxicity/Antitoxicity assays

The toxicity of AbiEii was determined as previously described [7] using an inducible expression plasmid containing the toxin gene, *abiEii,* under the control of the stringent *araBAD* promoter [52]. Using this setup, expression of AbiEii is repressed in the presence of glucose and inducible with the addition of arabinose [7,52]. For antitoxicity assays, the AbiEi expression constructs, under control of the T5/Lac promoter, were tested for their ability to abrogate AbiEii-mediated toxicity. *E. coli* cultures were grown overnight in a Labcon deep 96 square well plate at 12,000 rpm at 37°C using an orbital plate shaker (IncuMix, BioProducts). These were subcultured into a fresh deep well plate containing 1.2 ml LB, Ap, Sp and glu per well at a starting OD_{600} of 0.05. After 3 h of growth at 37°C with shaking at 12,000 rpm, bacteria were pelleted, washed twice and a dilution series was performed in phosphate buffered saline (PBS). Toxicity was quantitated by plating the dilution series onto LBA, Ap, Sp plates supplemented with: *i*. glu only; *ii.* ara only and *iii.* ara and IPTG. After overnight incubation at 37°C the colony forming units (CFU) were determined for each treatment and the antitoxicity activity determined as $[\log(CFU_{+ara+IPTG}) - \log(CFU_{+ara})]/[\log(CFU_{+glu})-\log(CFU_{+ara})] \times 100\%$. The antitoxicity activity in the absence of AbiEi expression (-ve control) is, by definition, 0%.

Protein expression and purification

Briefly, *E. coli* BL21, pPF1087 (His_6-Linker-TEV-AbiE, or a plasmid containing a SDM in AbiEi), pRARE was grown with LB and Ap, subcultured 1:100 in 100 ml in 1 L flasks and grown at 25°C at 200 rpm. For expression of some SDMs (from plasmids pPF1221 (R44A:R66A), pPF1225 (K69A) and pPF1226 (R97A)) an *E. coli* BW25116 Δ*lon*, pRARE strain was used to increase yield. When an OD_{600} of ~0.5 was reached, protein expression was induced with 1 mM IPTG and cultures were incubated overnight at 25°C at 200 rpm. Cells were harvested by centrifugation at 3,000 g at 4°C. The cell pellets were resuspended in 5 ml of equilibration buffer (10 mM HEPES-NaOH pH 7.5, 300 mM NaCl, 5 mM imidazole, and cOmplete mini EDTA-free protease inhibitor cocktail (Roche)). Cells were lysed by a total of 4 min sonication in 10 s pulses at an amplitude of 30%. The cell lysate was clarified by centrifugation at 10,000 g at 4°C for 15 min.

The clarified lysate was loaded on to a 1 ml bed volume of Ni-NTA resin (Protino) equilibrated with equilibration buffer. Unbound proteins were removed by washing with 20 column volumes of wash buffer (10 mM HEPES-NaOH pH 7.5, 300 mM NaCl, 20 mM imidazole) followed by 5 column volumes of low imidazole elution buffer (10 mM HEPES-NaOH pH 7.5, 300 mM NaCl, 75 mM imidazole). Proteins bound to the resin were eluted using 5 column volumes of high imidazole elution buffer (10 mM HEPES-NaOH pH 7.5, 300 mM NaCl, 250 mM imidazole). Fractions were analyzed on 12% SDS-PAGE gels by Coomassie blue stain. Fractions of interest were pooled into dialysis tubing (SnakeSkin, 3500 MWCO, Thermo Scientific) and TEV protease was added. Samples were then dialyzed overnight in 10 mM HEPES-NaOH, pH 7.5, 300 mM NaCl, 5 mM imidazole and 1 mM DTT

(dialysis buffer). To remove the cleaved His_6 tag, post-cleavage samples were run over a 1 ml bed volume of Ni-NTA resin (Protino) using 5 bed volumes of wash buffer. Fractions were analyzed on 12% SDS-PAGE gels by Coomassie blue stain. Fractions of interest were concentrated down to 500 µl using Ultra 4 Centrifugal filters, Ultracel 10K (Amicon). Concentrated samples had 250 µl of storage buffer added (10 mM HEPES, 150 mM NaCl, 70% (v/v) glycerol). Aliquots of protein were then snap frozen using dry ice and ethanol and stored at -80°C.

Electrophoretic Mobility Shift Assays

A 175 bp promoter region was amplified by PCR using primers PF1150 and PF2081 (5' IRDye® 700) for fluorescently labeled DNA, and PF1150 and PF2178 for unlabeled DNA. The templates contained either the native promoter region with both inverted repeats (pRLD32) or mutated versions lacking one or both of the predicted AbiEi binding sites (pRLD65, pRLD67 or pRLD68). A short fluorescent duplex (PF2379) was used for the 23 bp operator probe. For the probe containing a spacer between the two operator sites a gBlock (PF2380, Integrated DNA Technologies) was used as template for PCR. All DNA substrates were gel purified and the AbiEi proteins were purified as described above. Binding reactions contained 8 µl binding buffer (5 mM HEPES pH 7.6, 0.25 mM EDTA, 2.5 mM $(NH_4)_2SO_4$, 0.25 mM DTT, 0.05% (w/v) Tween 20, 7.5 mM KCl, 3.1 mM $MgCl_2$, 0.5 µg Poly[d(I-C)] (Roche), 50 ng Poly L-lysine (Roche), 10 µg BSA), 1 µl fluorescently labeled DNA (35 fmol) and 1 µl AbiEi protein diluted with dialysis buffer. For assays involving specific (native promoter) and non-specific (promoter with both binding sites mutated) competition, 100-fold excess unlabeled DNA (3.5 pmol) was included. Reactions were incubated at room temperature for 15 min and then run on 0.5X TBE 6% polyacrylamide gels

(4% polyacrylamide gels for probe containing a spacer) at 200 V and 4ºC. Fluorescence was measured using the Odyssey^{R} Fc Dual mode imaging system (LI-COR) at 700 nm. Bands intensities were quantified using Image Systems software (LI-COR) and were used to determine the proportion of occupied DNA binding sites (Y). Apparent dissociation constants (*Kd*) were determined from nonlinear regression fits of the data according to a single site binding model in GraphPad Prism version 6.0. The *Kd* was derived from the following equation $Kd = [P]^{nH}((1-Y)/Y)$, where *Kd* is the apparent dissociation constant, [P] is the protein concentration, *nH* is the Hill constant, and Y is the proportion of occupied binding sites. The Hill constant is the gradient of the Hill plot slope and was determined using GraphPad Prism version 6.0. Mean and standard error of the mean (SEM) values are derived from at least three independent experiments.

DNA bending assays

Equal sized DNA fragments containing the two AbiE IRs were generated by PCR using pPF1401 as a template and the following primer pairs; PF2839 and PF2840, PF2841 and PF2842, PF2843 and PF2844, PF2845 and PF2846, and PF2847 and PF2848. DNA fragments were gel purified and resulted in five DNA fragments containing the AbiEi IRs positioned differently with respects to the ends. Binding reactions contained 8 µl binding buffer (5 mM HEPES pH 7.6, 0.25 mM EDTA, 2.5 mM $(NH_4)_2SO_4$, 0.25 mM DTT, 0.05% (w/v) Tween 20, 7.5 mM KCl, 3.1 mM $MgCl_2$, 10 µg BSA), 1 µl template DNA (36.3 fmol) and 50 nM AbiEi protein diluted with dialysis buffer. Reactions were incubated at room temperature for 15 min and then run on 0.5X TBE 6% polyacrylamide gels at 200 V and 4ºC. Gels were stained for 15 min in SYBR gold, and then imaged using the Odyssey^{R} Fc Dual mode imaging

system (LI-COR) at 600 nm. The relative mobility of DNA fragments with or without protein was used to estimate the bend angle, α, using the formulae, $a = -b = 2c\,(1-\cos\alpha)$ as previously described [53].

Acknowledgements

This work was supported by a Rutherford Discovery Fellowship (PCF) from the Royal Society of New Zealand (RSNZ) the Marsden Fund, RSNZ, a University of Otago Research Grant, a Deans Bequest Fund from the School of Biomedical Sciences and a University of Otago's Matariki Network of Universities' (MNU) Travel Award between Otago and Durham Universities. HGH was supported by a University of Otago Doctoral Scholarship. We thank Manfred Weiss (Helmholtz-Zentrum Berlin, Germany) for sharing the coordinates of the model of *M. tuberculosis* Rv2827c bound to DNA.

References

[1] S. Chibani-Chennoufi, A. Bruttin, M.-L. Dillmann, H. Brüssow, Phage-Host Interaction: an Ecological Perspective, Journal of Bacteriology. 186 (2004) 3677–3686.

[2] K.E. Wommack, R.R. Colwell, Virioplankton: viruses in aquatic ecosystems, Microbiology and Molecular Biology Reviews. 64 (2000) 69–114.

[3] R.L. Dy, C. Richter, G.P.C. Salmond, P.C. Fineran, Remarkable Mechanisms in Microbes to Resist Phage Infections, Annu. Rev. Virol. 1 (2014) 307–331.

[4] S.J. Labrie, J.E. Samson, S. Moineau, Bacteriophage resistance mechanisms, Nat. Rev. Microbiol. 8 (2010) 317–327.

[5] M.-C. Chopin, A. Chopin, E. Bidnenko, Phage abortive infection in lactococci: variations on a theme, Current Opinion in Microbiology. 8 (2005) 473–479.

[6] M. Fukuyo, A. Sasaki, I. Kobayashi, Success of a suicidal defense strategy against infection in a structured habitat, Sci. Rep. 2 (2012) 1828.

[7] R.L. Dy, R. Przybilski, K. Semeijn, G.P.C. Salmond, P.C. Fineran, A widespread bacteriophage abortive infection system functions through a Type IV toxin–antitoxin mechanism, Nucleic Acids Research. 42 (2014) 4590–4605.

[8] P.C. Fineran, T.R. Blower, I.J. Foulds, D.P. Humphreys, K.S. Lilley, G.P.C. Salmond, The phage abortive infection system, ToxIN, functions as a protein-RNA toxin-antitoxin pair, Proceedings of the National Academy of Sciences. 106 (2009) 894–899.

[9] J.E. Samson, S. Spinelli, C. Cambillau, S. Moineau, Structure and activity of AbiQ, a lactococcal endoribonuclease belonging to the type III toxin-antitoxin system, Molecular Microbiology. 87 (2013) 756–768.

[10] D.C. Pecota, T.K. Wood, Exclusion of T4 phage by the *hok/sok* killer locus from plasmid R1, Journal of Bacteriology. 178 (1996) 2044–2050.

[11] R. Hazan, H. Engelberg-Kulka, *Escherichia coli mazEF*-mediated cell death as a defense mechanism that inhibits the spread of phage P1, Mol Genet Genomics. 272 (2004) 227–234.

[12] K. Gerdes, J.E. Larsen, S. Molin, Stable inheritance of plasmid R1 requires two different loci, Journal of Bacteriology. 161 (1985) 292–298.

[13] T. Ogura, S. Hiraga, Mini-F plasmid genes that couple host cell division to plasmid proliferation, Proceedings of the National Academy of Sciences. 80 (1983) 4784–4788.

[14] G.M. Cook, J.R. Robson, R.A. Frampton, J. McKenzie, R. Przybilski, P.C. Fineran, et al., Ribonucleases in bacterial toxin–antitoxin systems, Biochimica Et Biophysica Acta (BBA) - Gene Regulatory Mechanisms. 1829 (2013) 523–531.

[15] K. Gerdes, E. Maisonneuve, Bacterial Persistence and Toxin-Antitoxin Loci, Annu. Rev. Microbiol. 66 (2012) 103–123.

[16] R. Page, W. Peti, Toxin-antitoxin systems in bacterial growth arrest and persistence, Nat Chem Biol. 12 (2016) 208–214.

[17] E.M. Fozo, M.R. Hemm, G. Storz, Small Toxic Proteins and the Antisense RNAs That Repress Them, Microbiology and Molecular Biology Reviews. 72 (2008) 579–589.

[18] R. Leplae, D. Geeraerts, R. Hallez, J. Guglielmini, P. Drèze, L. Van Melderen, Diversity of bacterial type II toxin–antitoxin systems: a comprehensive search and functional analysis of novel families, Nucleic Acids Research. 39 (2011) 5513–5525.

[19] E. Aizenman, H. Engelberg-Kulka, G. Glaser, An *Escherichia coli* chromosomal "addiction module" regulated by guanosine [corrected] 3“,5-”bispyrophosphate: a model for programmed bacterial cell death, Proceedings of the National Academy of Sciences. 93 (1996) 6059–6063.

[20] T.R. Blower, X.Y. Pei, F.L. Short, P.C. Fineran, D.P. Humphreys, B.F. Luisi, et al., A processed noncoding RNA regulates an altruistic bacterial antiviral system, Nat Struct Mol Biol. 18 (2011) 185–190.

[21] H. Masuda, Q. Tan, N. Awano, K.-P. Wu, M. Inouye, YeeU enhances the bundling of cytoskeletal polymers of MreB and FtsZ, antagonizing the CbtA (YeeV) toxicity in *Escherichia coli*, Molecular Microbiology. 84 (2012) 979–989.

[22] H. Masuda, Q. Tan, N. Awano, Y. Yamaguchi, M. Inouye, A novel membrane-bound toxin for cell division, CptA (YgfX), inhibits polymerization of cytoskeleton proteins, FtsZ and MreB, in *Escherichia coli*, FEMS Microbiol Lett. 328 (2012) 174–181.

[23] X. Wang, D.M. Lord, H.-Y. Cheng, D.O. Osbourne, S.H. Hong, V. Sanchez-Torres, et al., A new type V toxin-antitoxin system where mRNA for toxin GhoT is cleaved by antitoxin GhoS, Nat Chem Biol. 8 (2012) 855–861.

[24] C.D. Aakre, T.N. Phung, D. Huang, M.T. Laub, A Bacterial Toxin Inhibits DNA Replication Elongation through a Direct Interaction with the β Sliding Clamp, Molecular Cell. 52 (2013) 617–628.

[25] P. Garvey, G.F. Fitzgerald, C. Hill, Cloning and DNA sequence analysis of two abortive infection phage resistance determinants from the lactococcal plasmid pNP40, Applied and Environmental Microbiology. 61 (1995) 4321–4328.

[26] K. Kuchta, L. Knizewski, L.S. Wyrwicz, L. Rychlewski, K. Ginalski, Comprehensive classification of nucleotidyltransferase fold proteins: identification of novel families and their representatives in human, Nucleic Acids Research. 37 (2009) 7701–7714.

[27] H. Sberro, A. Leavitt, R. Kiro, E. Koh, Y. Peleg, U. Qimron, et al., Discovery of Functional Toxin/Antitoxin Systems in Bacteria by Shotgun Cloning, Molecular Cell. 50 (2013) 136–148.

[28] R.A.F. Wozniak, M.K. Waldor, A Toxin–Antitoxin System Promotes the Maintenance of an Integrative Conjugative Element, PLoS Genet. 5 (2009) e1000439. doi:10.1371/journal.pgen.1000439.

[29] R. Janowski, S. Panjikar, A.N. Eddine, S.H.E. Kaufmann, M.S. Weiss, Structural analysis reveals DNA binding properties of Rv2827c, a hypothetical protein from *Mycobacterium tuberculosis*, J Struct Funct Genomics. 10 (2009) 137–150.

[30] M. Overgaard, J. Borch, M.G. Jørgensen, K. Gerdes, Messenger RNA interferase RelE controls *relBE* transcription by conditional cooperativity, Molecular Microbiology. 69 (2008) 841–857.

[31] K. Gerdes, S.K. Christensen, A. Løbner-Olesen, Prokaryotic toxin-antitoxin stress response loci, Nat. Rev. Microbiol. 3 (2005) 371–382.

[32] F. Hayes, B. Kędzierska, Regulating toxin-antitoxin expression: controlled detonation of intracellular molecular timebombs, Toxins. 6 (2014) 337–358.
[33] L.A. Kelley, S. Mezulis, C.M. Yates, M.N. Wass, M.J.E. Sternberg, The Phyre2 web portal for protein modeling, prediction and analysis, Nat Protoc. 10 (2015) 845–858.
[34] R.G. Brennan, B.W. Matthews, The helix-turn-helix DNA binding motif, J. Biol. Chem. 264 (1989) 1903–1906.
[35] R.G. Brennan, The winged-helix DNA-binding motif: Another helix-turn-helix takeoff, Cell. 74 (1993) 773–776.
[36] L. Aravind, V. Anantharaman, S. Balaji, M. Babu, L. Iyer, The many faces of the helix-turn-helix domain: Transcription regulation and beyond, FEMS Microbiol. Rev. 29 (2005) 231–262.
[37] D. Lobato-Márquez, R. Díaz-Orejas, F. García-Del Portillo, Toxin-antitoxins and bacterial virulence, FEMS Microbiol. Rev. 40 (2016) 592–609.
[38] M.A. Schumacher, K.M. Piro, W. Xu, S. Hansen, K. Lewis, R.G. Brennan, Molecular Mechanisms of HipA-Mediated Multidrug Tolerance and Its Neutralization by HipB, Science. 323 (2009) 396–401.
[39] R. Loris, A. Garcia-Pino, Disorder- and dynamics-based regulatory mechanisms in toxin-antitoxin modules, Chem. Rev. 114 (2014) 6933–6947.
[40] A. Garcia-Pino, S. Balasubramanian, L. Wyns, E. Gazit, H. De Greve, R.D. Magnuson, et al., Allostery and Intrinsic Disorder Mediate Transcription Regulation by Conditional Cooperativity, Cell. 142 (2010) 101–111.
[41] M.V. Merfa, B. Niza, M.A. Takita, A.A. De Souza, The MqsRA Toxin-Antitoxin System from Xylella fastidiosa Plays a Key Role in Bacterial Fitness, Pathogenicity, and Persister Cell Formation, Front. Microbiol. 7 (2016) 841.
[42] V.W.C. Soo, T.K. Wood, Antitoxin MqsA Represses Curli Formation Through the Master Biofilm Regulator CsgD, Sci. Rep. 3 (2013) 711.
[43] X. Wang, T.K. Wood, Toxin-Antitoxin Systems Influence Biofilm and Persister Cell Formation and the General Stress Response, Applied and Environmental Microbiology. 77 (2011) 5577–5583.
[44] C.M. Sassetti, D.H. Boyd, E.J. Rubin, Genes required for mycobacterial growth defined by high density mutagenesis, Molecular Microbiology. 48 (2003) 77–84.
[45] A. Gupta, B. Venkataraman, M. Vasudevan, K. Gopinath Bankar, Co-expression network analysis of toxin-antitoxin loci in *Mycobacterium tuberculosis* reveals key modulators of cellular stress, Sci. Rep. 7 (2017) 5868.
[46] M. Haenni, E. Saras, S. Bertin, P. Leblond, J.-Y. Madec, S. Payot, Diversity and Mobility of Integrative and Conjugative Elements in Bovine Isolates of Streptococcus *agalactiae*, *S. dysgalactiae* subsp. *dysgalactiae*, and *S. uberis*, Applied and Environmental Microbiology. 76 (2010) 7957–7965.
[47] M. Kearse, R. Moir, A. Wilson, S. Stones-Havas, M. Cheung, S. Sturrock, et al., Geneious Basic: An integrated and extendable desktop software

platform for the organization and analysis of sequence data, Bioinformatics. 28 (2012) 1647–1649.

[48] S.F. Altschul, W. Gish, W. Miller, E.W. Myers, D.J. Lipman, Basic local alignment search tool, Journal of Molecular Biology. 215 (1990) 403–410.

[49] N.A. Baker, D. Sept, S. Joseph, M.J. Holst, J.A. McCammon, Electrostatics of nanosystems: application to microtubules and the ribosome, Proceedings of the National Academy of Sciences. 98 (2001) 10037–10041.

[50] J.P. Ramsay, High-throughput β-Galactosidase and β-Glucuronidase Assays Using Fluorogenic Substrates, Bio-Protocol. 3 (2013) 1–7.

[51] A.G. Patterson, J.T. Chang, C. Taylor, P.C. Fineran, Regulation of the Type I-F CRISPR-Cas system by CRP-cAMP and GalM controls spacer acquisition and interference, Nucleic Acids Research. 43 (2015) 6038–6048.

[52] L.M. Guzman, D. Belin, M.J. Carson, J. Beckwith, Tight regulation, modulation, and high-level expression by vectors containing the arabinose P_{BAD} promoter, Journal of Bacteriology. 177 (1995) 4121–4130.

[53] I. Papapanagiotou, S.D. Streeter, P.D. Cary, G.G. Kneale, DNA structural deformations in the interaction of the controller protein C.AhdI with its operator sequence, Nucleic Acids Research. 35 (2007) 2643–2650.

Figure Legends

Fig. 1. The positively charged surface of AbiEi. (A) Solvent-accessible electrostatic surface of the *M. tuberculosis* AbiEi homologue, Rv2827c (PDB:1ZEL), coloured by electrostatic potential (blue is positive and red negative). (B) Solvent-accessible surface of the *S. agalactiae* AbiEi model structure, coloured by electrostatic potential, showing the predicted DNA-binding positively charged (blue) surface and opposing, negatively charged (red) face. Note that the final 41 resides of the CTD could not be confidently modelled. (C) Phyre2-generated sequence alignment between AbiEi and Rv2827c, used to generate the AbiEi model, showing the predicted secondary structure for AbiEi. Residues that were selected for mutagenesis are coloured either orange (lysine) or green (arginine). (D) The predicted DNA-binding face of AbiEi with mutated residues coloured as in (C). (E) Model for the interaction of the wHTH domain of AbiEi with DNA, based on Janowski *et al* 2009 [29] with mutated residues coloured as in (C).

Fig. 2. Autoregulation and antitoxicity for the surface charge depleted single mutants. (A) Schematic of AbiE inverted repeats 1 and 2 (IR1, IR2), with regards to the -35, -10, ribosome binding sites (RBS) and the start codon (M). Solid arrow shows the conserved 11 bp, while dotted arrow shows the partially conserved regions of the inverted repeats. Sequence differences between the partially conserved regions are shown in red. (B) Schematic of the autoregulation assay, showing AbiEi binding the *abiE* operator inverted repeats and suppressing *lacZ* expression. (C) Autoregulation by single alanine substitution mutants of AbiEi, measured using a *lacZ* reporter assay. The β-gal activity observed for each mutant was normalized to the non-repressed *abiE* promoter activity observed in the absence of AbiEi (-ve). (D) Schematic of the antitoxicity assay. (E) Antitoxicity capability of WT AbiEi and each of the single mutants. Data shown are the means and error bars represent the SEM (*n*=3).

Fig. 3. The positively charged face of the CTD is required for negative autoregulation. (A) Autoregulation by the double and triple mutants of AbiEi, measured using a *lacZ* reporter assay as described in Fig. 2 (B) Antitoxicity

capability of WT AbiEi and each of the double and triple mutants. Data shown are the means and error bars represent the SEM (*n*=3).

Fig. 4. AbiEi cooperatively binds and bends the *abiE* operator. Electrophoretic mobility shift assays performed using WT AbiEi, with a fluorescently labeled probe containing either (A) the native *abiE* promoter region, or mutated operator sequences where either (B) IR1, (C) IR2 or (D) both IR1 and IR2 were replaced by cytosines. The schematics to the right of each gel image depict the DNA constructs used in each experiment. The concentration of AbiEi was increased from 0.78 to 50 nM in 2-fold steps. The labels indicate (N) non-shifted, (1) single shifted and (2) double shifted bands. The lanes denoted (S) and (NS) indicate competition by 100-fold molar excess of unlabeled specific DNA or non-specific DNA, respectively, with 25 nM AbiEi. The (E) binding curve, (F) Hill plot and (G) Scatchard plot for the interaction of AbiEi with the native *abiE* promoter, as represented in (A). EMSAs were carried out using a short fluorescent probe, (H) containing only one inverted repeat, and (I) using a probe with a 50 bp spacer inserted between the two inverted repeats. The (J) binding curve, (K) Hill plot and (L) Scatchard plot for the interaction of AbiEi with the fluorescent probe containing a linker between the inverted repeats as seen in (I). (M) a representative DNA bending assay using WT AbiEi at 50 nM. Schematic shows the DNA probe in black, with the relative IR location in red. (N) The DNA bending curve shows the relative mobility of the fragments based on the location of the AbiEi binding sites and was used to calculate the bending angles. All EMSAs were performed at least three times, graphs and error bars represent the mean ± SEM.

Fig. 5. Impaired DNA binding by the AbiEi mutants. Electrophoretic mobility shift assays were performed using either WT AbiEi or the (A) specified single or (B) double mutants with a fluorescently labeled probe comprising the native *abiE* promoter region. The (C) R100A and (D) R97A mutants were also tested in EMSAs when either IR1 or IR2 were replaced with cytosines. The labels indicate (N) non-shifted or (1) single shifted. The concentration of AbiEi was increased from 0.78 up to 50 nM in 2-fold steps. Apparent *Kd* values are the mean ± SEM (n=3). The label

cooperative indicates AbiEi binding is cooperative and ND indicates no *Kd* could be calculated. Refer to Fig. S2 for *Kd* curves, Hill and Scatchard plots.

Fig. 6. Model for AbiEi autoregulation via binding to IRs in the *abiE* promoter region. Binding of one AbiEi monomer to IR1 or IR2 has an apparent *Kd* of 7.9 ± 1.2 or 7.4 ± 1.2 respectively. The NTD binds to the highly conserved 11 bp (black boxes) with the CTD binding to the lesser conserved region containing 4 mismatches (grey boxes). The binding of a second AbiEi is cooperative (i.e. increased likelihood following the binding of the first AbiEi monomer), and this exhibits an apparent *Kd* of 10.8 ± 0.7. This results in a bend in the DNA of 72° ± 2°, and also the transcriptional repression of the AbiEi operator, most likely due occlusion of the RNA polymerase through blocking the -35 and -10 promoter elements.

Table 1. Plasmids used in this study

Plasmid	Genotype/Phenotype	Reference
pBAD30	*E. coli* arabinose inducible vector, Ap^R, pACYC184/p15A replicon	[39]
pTA100	pQE-80L derivative with Sm/Sp resistant cassette, Sm/Sp^R, ColE1 replicon	[8]
pRW50	Promoterless *lacZ* fusion plasmid, Tc^R, RK2 replicon	[53]
pRARE	*E. coli* rare tRNA, pACYC-184 derivative, Cm^R, p15A replicon	[54]
pRLD12	Native AbiEii, pBAD30-derivative, Ap^R	[7]
pRLD13	Native AbiEi, pTA100-derivative, Sm^R/Sp^R	[7]
pRLD32	P_{abiE} *lacZ* fusion (-72 to +50) pRW50 derivative, Tc^R	[7]
pRLD65	*S. agalactiae* V/R 2603 P_{abiE} 100bp, IR 1 replaced with C	[7]
pRLD67	*Streptococcus agalactiae* V/R 2603 P_{abiE} 100 bp, IR2 replaced with C	[7]
pRLD68	*Streptococcus agalactiae* V/R 2603 P_{abiE} 100 bp, IR1 and 2 replaced with C	[7]
pPF1067	pQE80L-oriT, N terminal His_6 with TEV cleavage site	This study
Untagged AbiEi SDMs		
pPF627	K3A AbiEi, pTA100-derivative, Sm^R/Sp^R	This study
pPF628	K4A AbiEi, pTA100-derivative, Sm^R/Sp^R	This study
pPF1145	K13A AbiEi, pTA100-derivative, Sm^R/Sp^R	This study
pPF629	K21A AbiEi, pTA100-derivative, Sm^R/Sp^R	This study
pPF630	K24A AbiEi, pTA100-derivative, Sm^R/Sp^R	This study
pPF665	R35A AbiEi, pTA100-derivative, Sm^R/Sp^R	This study
pPF631	K38A AbiEi, pTA100-derivative, Sm^R/Sp^R	This study
pPF632	R44A AbiEi, pTA100-derivative, Sm^R/Sp^R	This study
pPF633	K47A AbiEi, pTA100-derivative, Sm^R/Sp^R	This study
pPF634	R66A AbiEi, pTA100-derivative, Sm^R/Sp^R	This study
pPF635	K69A AbiEi, pTA100-derivative, Sm^R/Sp^R	This study
pPF1146	R97A AbiEi, pTA100-derivative, Sm^R/Sp^R	This study
pPF636	R100A AbiEi, pTA100-derivative, Sm^R/Sp^R	This study
pPF1147	K115A AbiEi, pTA100-derivative, Sm^R/Sp^R	This study
pPF637	R134A AbiEi, pTA100-derivative, Sm^R/Sp^R	This study
pPF1148	R149A AbiEi, pTA100-derivative, Sm^R/Sp^R	This study
pPF1149	K151A AbiEi, pTA100-derivative, Sm^R/Sp^R	This study
pPF668	K159A AbiEi, pTA100-derivative, Sm^R/Sp^R	This study
pPF669	K169A AbiEi, pTA100-derivative, Sm^R/Sp^R	This study
pPF670	K170A AbiEi, pTA100-derivative, Sm^R/Sp^R	This study
pPF671	K174A AbiEi, pTA100-derivative, Sm^R/Sp^R	This study
pPF672	K181A AbiEi, pTA100-derivative, Sm^R/Sp^R	This study
pPF673	K187A AbiEi, pTA100-derivative, Sm^R/Sp^R	This study

pPF674	K189A AbiEi, pTA100-derivative, Sm^R/Sp^R	This study
pPF701	R44A:R100A AbiEi, pTA100-derivative, Sm^R/Sp^R	This study
pPF702	R44A:R66A AbiEi, pTA100-derivative, Sm^R/Sp^R	This study
pPF757	K159A:K170A AbiEi, pTA100-derivative, Sm^R/Sp^R	This study
pPF759	K170A:K181A AbiEi, pTA100-derivative, Sm^R/Sp^R	This study
pPF761	K181A:K189A AbiEi, pTA100-derivative, Sm^R/Sp^R	This study
pPF764	R66A:R100A AbiEi, pTA100-derivative, Sm^R/Sp^R	This study
pPF768	K170A:K181A:K189A AbiEi, pTA100-derivative, Sm^R/Sp^R	This study
pPF1308	K69A:R100A AbiEi, pTA100-derivative Sm^R/Sp^R	This study
pPF1309	K69A:R97A AbiEi, pTA100-derivative Sm^R/Sp^R	This study
pPF1248	R97A:R100A AbiEi, pTA100-derivative Sm^R/Sp^R	This study
pPF1402	R44A:R66A:R100A AbiEi, pTA100-derivative Sm^R/Sp^R	This study
AbiEi overexpression constructs		
pPF1080	Native AbiEi, pPF1067 derivative, Ap^R	This study
pPF1140	R35A AbiEi, pPF1067 derivative, Ap^R	This study
pPF1141	R66A AbiEi, pPF1067 derivative, Ap^R	This study
pPF1142	R100A AbiEi, pPF1067 derivative, Ap^R	This study
pPF1143	R140A AbiEi, pPF1067 derivative, Ap^R	This study
pPF1144	R66A:R100A AbiEi, pPF1067 derivative, Ap^R	This study
pPF1221	R44A AbiEi, pPF1067 derivative, Ap^R	This study
pPF1222	K47A AbiEi, pPF1067 derivative, Ap^R	This study
pPF1223	K69A AbiEi, pPF1067 derivative, Ap^R	This study
pPF1224	R97A AbiEi, pPF1067 derivative, Ap^R	This study
pPF1225	R44A:R66A AbiEi, pPF1067 derivative, Ap^R	This study
pPF1226	R44A:R100A AbiEi, pPF1067 derivative, Ap^R	This study
pPF1401	pBend5 containing IR1 and IR2, Ap^R	

Highlights

- The Type IV antitoxin AbiEi has a positive surface charge that aids DNA binding
- AbiEi binds cooperatively to two inverted repeats overlapping the *abiE* promoter
- The AbiEi C-terminal domain binds to the extended region of the inverted repeats
- AbiEi binding causes DNA bending and repression of the *abiE* toxin-antitoxin operon

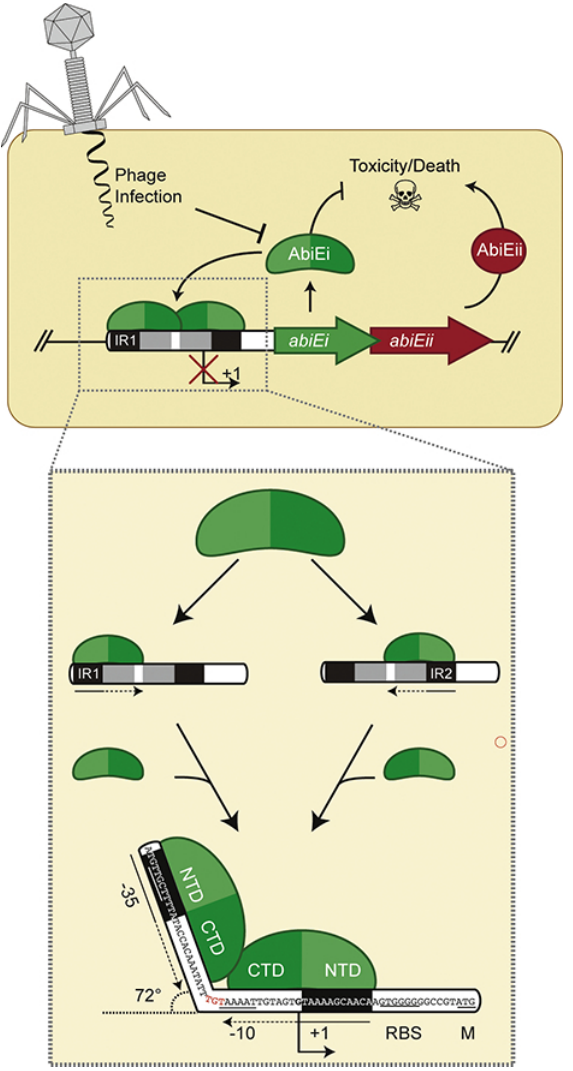

Graphics Abstract

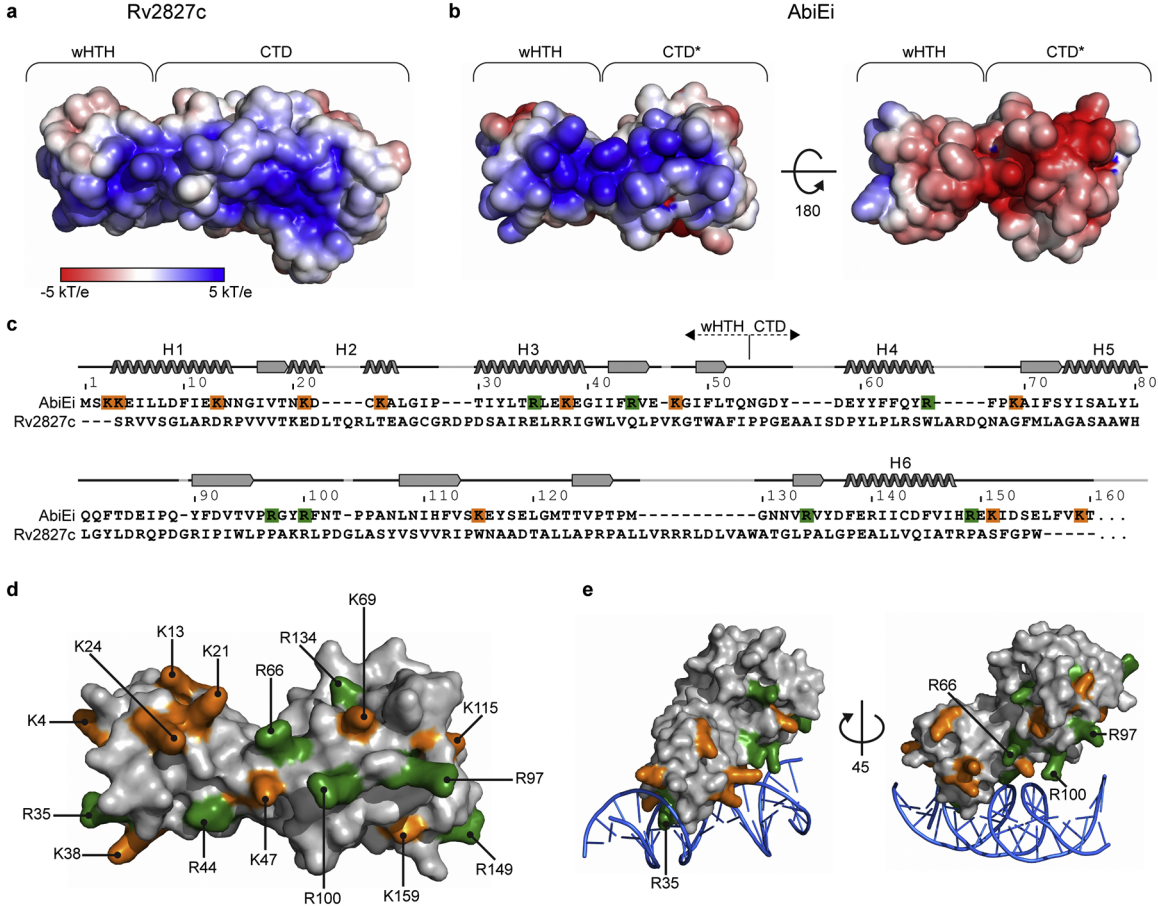
a
Rv2827c
wHTH
CTD
-5 kT/e
5 kT/e
b
AbiEi
wHTH
CTD*
180
c
wHTH CTD
H1
H2
H3
H4
H5
H6
AbiEi MSKKEILLDFIEKNNGIVTNKD----CKALGIP---TIYLTRLEKEGIIFRVE-KGIFLTQNGDY----DEYYFFQYR-----FPKAIFSYISALYL
Rv2827c ---SRVVSGLARDRPVVVTKEDLTQRLTEAGCGRDPDSAIRELRRIGWLVQLPVKGTWAFIPPGEAAISDPYLPLRSWLARDQNAGFMLAGASAAWH
AbiEi QQFTDEIPQ-YFDVTVPKGYRFNT-PPANLNIHFVSKEYSELGMTTVPTPM----------GNNVRVYDFERIICDFVIHKEKIDSELFVKT...
Rv2827c LGYLDRQPDGRIPIWLPPAKRLPDGLASYVSVVRIPWNAADTALLAPRPALLVRRRLDLVAWATGLPALGPEALLVQIATRPASFGPW-----...
d
K69
K13
K24
K21
R134
R66
K4
K115
R97
R35
K38
R44
K47
R149
R100
K159
e
R66
R97
45
R100
R35

Figure 1

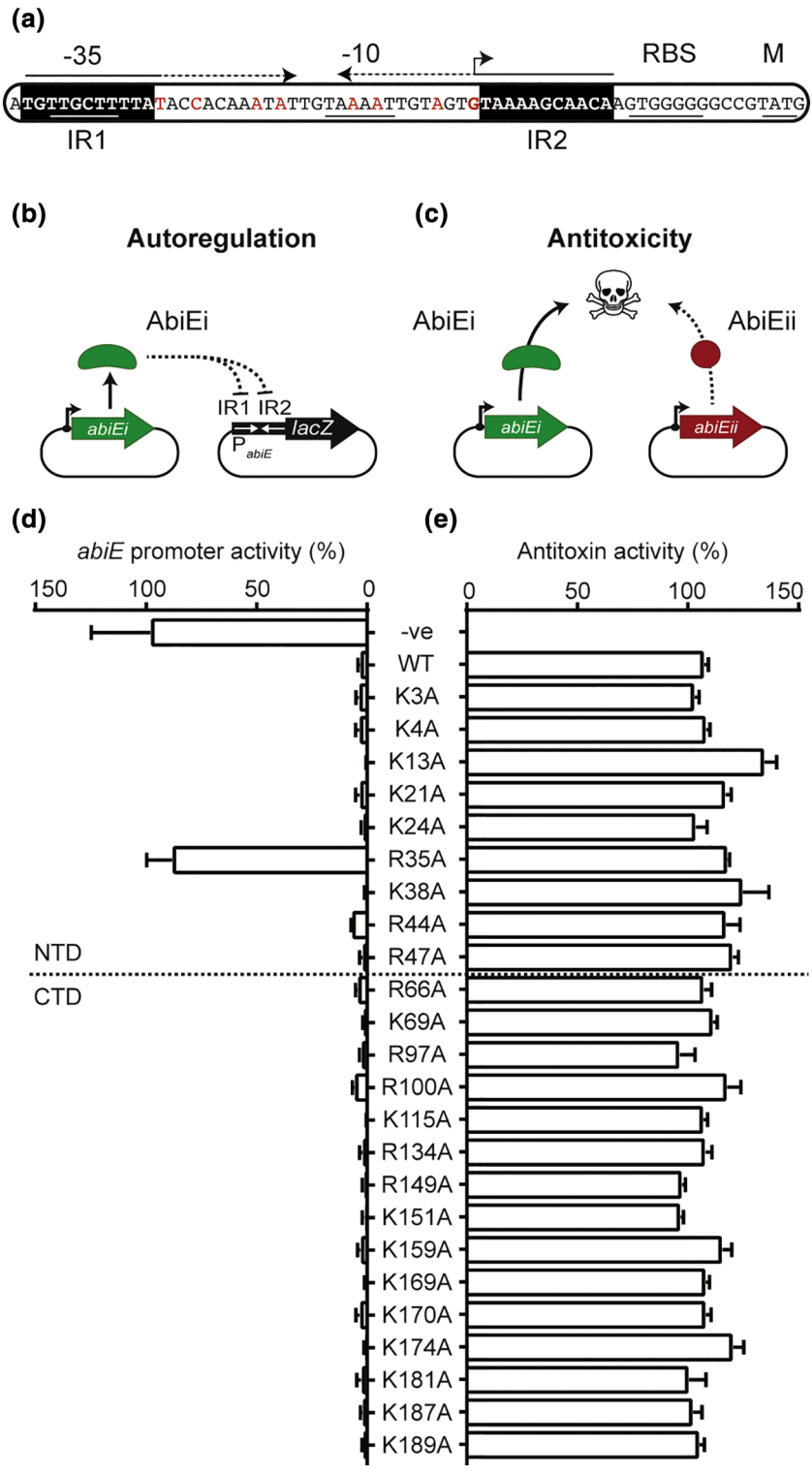
(a)
-35
-10
RBS
M
ATGTTGCTTTTATACCACAAATATTGTAAAATTGTAGTGTAAAAGCAACAAGTGGGGGGCCGTATG
IR1
IR2
(b)
Autoregulation
AbiEi
IR1 IR2
abiEi
lacZ
P abiE
(c)
Antitoxicity
AbiEi
AbiEii
abiEi
abiEii
(d)
abiE promoter activity (%)
150
100
50
0
(e)
Antitoxin activity (%)
0
50
100
150
-ve
WT
K3A
K4A
K13A
K21A
K24A
R35A
K38A
R44A
R47A
NTD
CTD
R66A
K69A
R97A
R100A
K115A
R134A
R149A
K151A
K159A
K169A
K170A
K174A
K181A
K187A
K189A

Figure 2

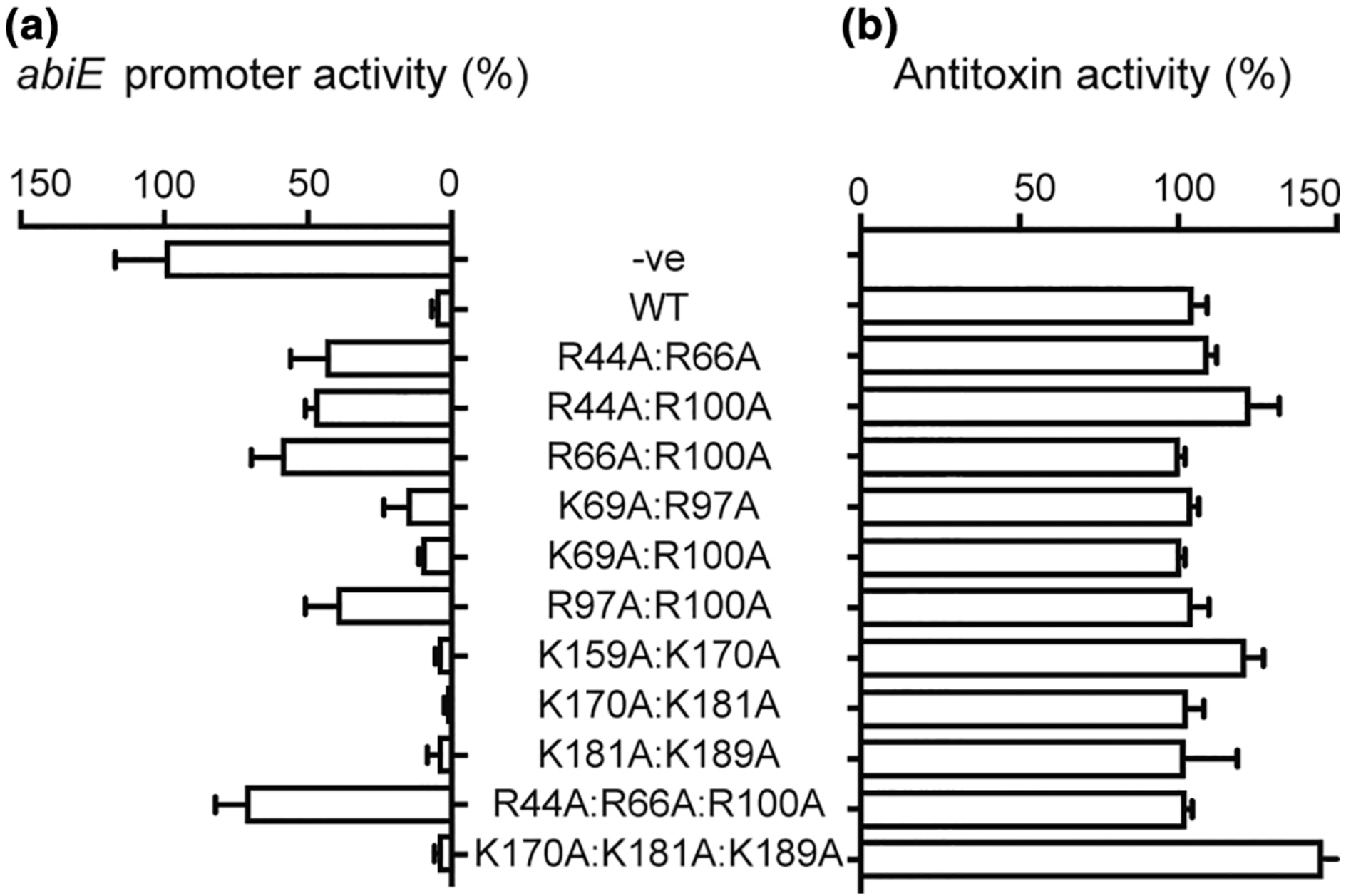
(a)
abiE promoter activity (%)
150
100
50
0
(b)
Antitoxin activity (%)
0
50
100
150
-ve
WT
R44A:R66A
R44A:R100A
R66A:R100A
K69A:R97A
K69A:R100A
R97A:R100A
K159A:K170A
K170A:K181A
K181A:K189A
R44A:R66A:R100A
K170A:K181A:K189A

Figure 3

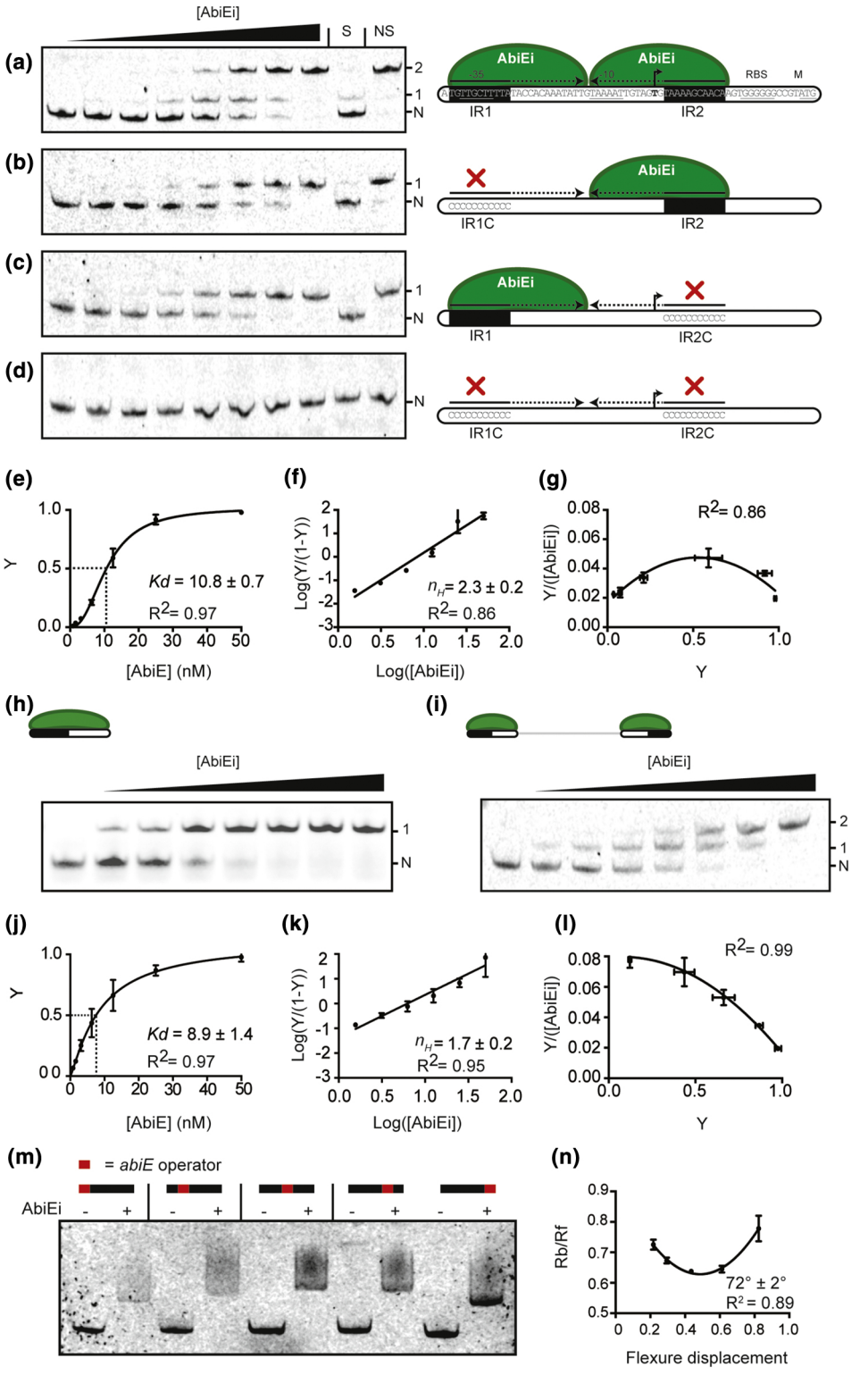
[AbiEi]
S
NS
(a)
(b)
(c)
(d)
2
1
N
AbiEi
-35
-10
RBS
M
IR1
IR2
IR1C
IR2C
(e)
Y
Kd = 10.8 ± 0.7
R2= 0.97
[AbiEi] (nM)
(f)
Log(Y/(1-Y))
nH= 2.3 ± 0.2
R2= 0.86
Log([AbiEi])
(g)
R2= 0.86
Y/([AbiEi])
Y
(h)
(i)
(j)
Kd = 8.9 ± 1.4
R2= 0.97
(k)
nH= 1.7 ± 0.2
R2= 0.95
(l)
R2= 0.99
(m)
= abiE operator
AbiEi
(n)
Rb/Rf
72° ± 2°
R2 = 0.89
Flexure displacement

Figure 4

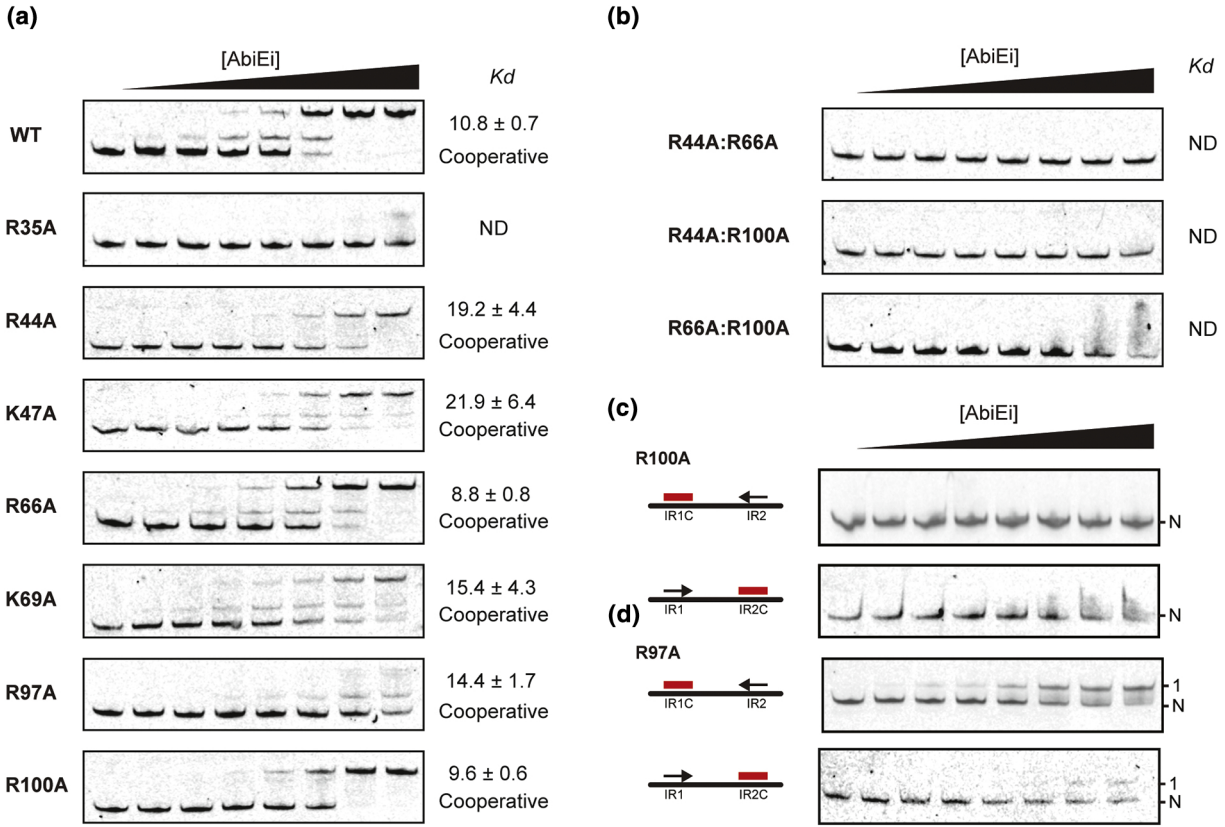
(a)
[AbiEi]
Kd
WT
10.8 ± 0.7
Cooperative
R35A
ND
R44A
19.2 ± 4.4
Cooperative
K47A
21.9 ± 6.4
Cooperative
R66A
8.8 ± 0.8
Cooperative
K69A
15.4 ± 4.3
Cooperative
R97A
14.4 ± 1.7
Cooperative
R100A
9.6 ± 0.6
Cooperative
(b)
[AbiEi]
Kd
R44A:R66A
ND
R44A:R100A
ND
R66A:R100A
ND
(c)
[AbiEi]
R100A
IR1C
IR2
N
IR1
IR2C
N
(d)
R97A
IR1C
IR2
1
N
IR1
IR2C
1
N

Figure 5

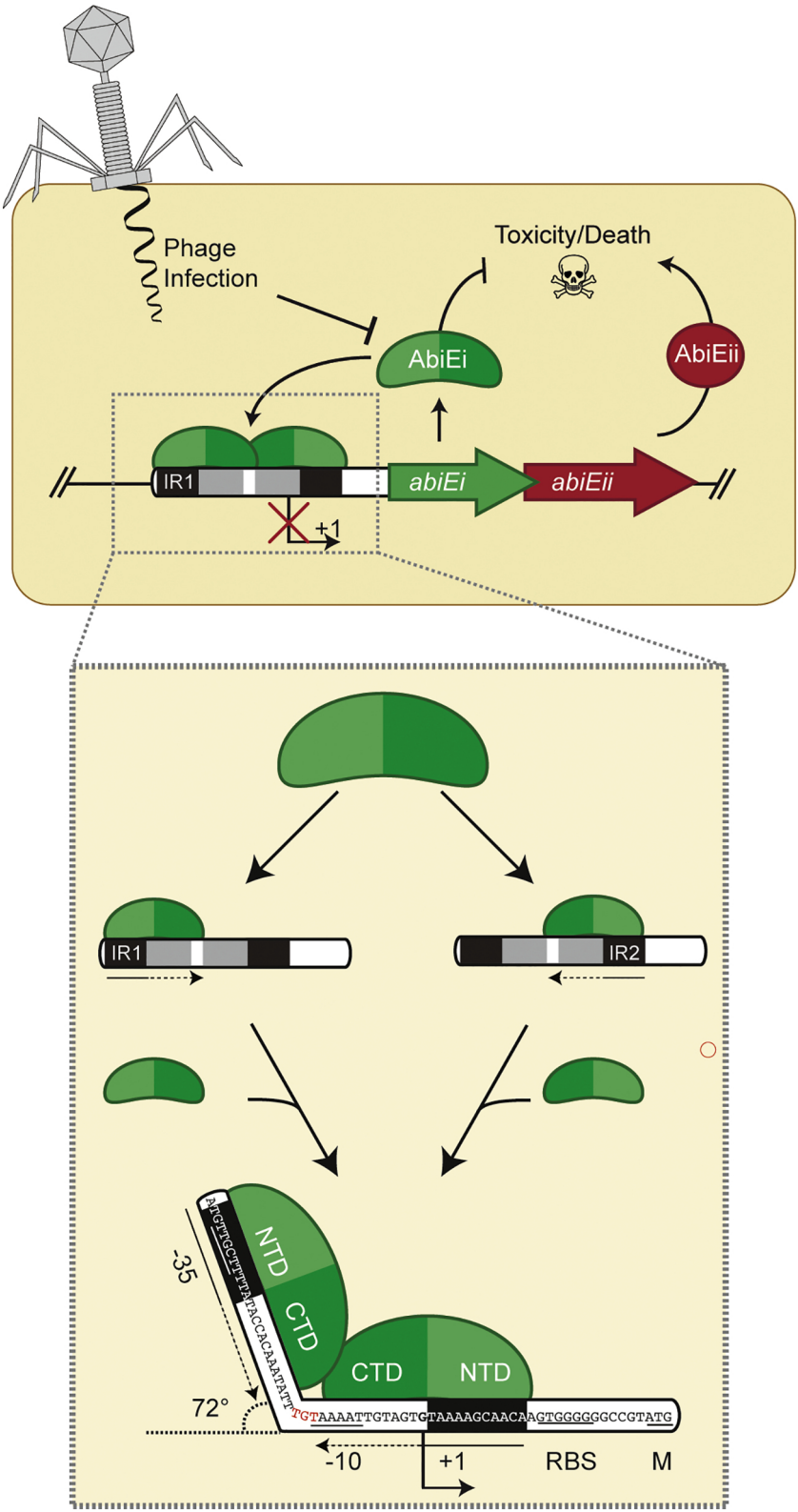
Phage
Infection
Toxicity/Death
AbiEi
AbiEii
IR1
abiEi
abiEii
+1
IR1
IR2
NTD
CTD
CTD
NTD
-35
72°
-10
+1
RBS
M

Figure 6